Antitumor effects of eribulin depend on modulation of the tumor microenvironment by vascular remodeling in mouse models

Ken Ito,[1,2] (iD) Shusei Hamamichi,[2] Takanori Abe,[1] Tsuyoshi Akagi,[1] Hiroshi Shirota,[1] Satoshi Kawano,[1] Makoto Asano,[3] Osamu Asano,[1] Akira Yokoi,[1] Junji Matsui,[3] Izumi O. Umeda[2] and Hirofumi Fujii[2]

[1]Halichondrin Research Laboratory, Eisai Co., Ltd, Tsukuba; [2]Division of Functional Imaging, National Cancer Center, Kashiwa; [3]Biology Research, Oncology, Eisai Co., Ltd., Tsukuba, Japan

We previously reported that eribulin mesylate (eribulin), a tubulin-binding drug (TBD), could remodel tumor vasculature (i.e. increase tumor vessels and perfusion) in human breast cancer xenograft models. However, the role of this vascular remodeling in antitumor effects is not fully understood. Here, we investigated the effects of eribulin-induced vascular remodeling on antitumor activities in multiple human cancer xenograft models. Microvessel densities (MVD) were evaluated by immunohistochemistry (CD31 staining), and antitumor effects were examined in 10 human cancer xenograft models. Eribulin significantly increased MVD compared to the controls in six out of 10 models with a correlation between enhanced MVD levels and antitumor effects (R^2 = 0.54). Because of increased MVD, we next used radiolabeled liposomes to examine whether eribulin treatment would result in increased tumoral accumulation levels of these macromolecules and, indeed, we found that eribulin, unlike vinorelbine (another TBD) enhanced them. As eribulin increased accumulation of radiolabeled liposomes, we postulated that this treatment might enhance the antitumor effect of Doxil (a liposomal anticancer agent) and facilitate recruitment of immune cells into the tumor. As expected, eribulin enhanced antitumor activity of Doxil in a post-erlotinib treatment H1650 (PE-H1650) xenograft model. Furthermore, infiltrating CD11b-positive immune cells were significantly increased in multiple eribulin-treated xenografted tumors, and natural killer (NK) cell depletion reduced the antitumor effects of eribulin. These findings suggest a contribution of the immune cells for antitumor activities of eribulin. Taken together, our results suggest that vascular remodeling induced by eribulin acts as a microenvironment modulator and, consequently, this alteration enhanced the antitumor effects of eribulin.

As microtubules are associated with multiple cellular mechanisms, they are recognized as promising targets for anticancer agents as evidenced by accumulating records demonstrating development of various microtubule-targeted drugs. However, corresponding binding sites of these microtubule-targeted drugs are unique;[1,2] hence, given the organization of the microtubule network in complex cellular activities,[3,4] tubulin inhibition through different binding sites may lead to a different mechanism of action (MOA). For example, eribulin, a non-taxane synthetic tubulin dynamics inhibitor, binds to a microtubule plus-end with high affinity, and thereby functions as a suppressor of microtubule dynamics.[5] On the contrary, vinorelbine, another tubulin-binding drug (TBD), binds to a vinca-binding domain of a β-tubulin subunit near the plus-end of the microtubule and functions as a microtubule destabilizer.[6] It is well-known that pharmacological effects of TBD are different to each other. Understanding the differences of MOA among these TBD would contribute to optimization of doses for antitumor regimens, and offer a unique opportunity for treatment strategy.

Eribulin is currently used in many countries to treat patients with late-stage, advanced or metastatic breast cancer, and liposarcoma.[7–10] Accumulating literature evidence suggests that eribulin induces unique cellular phenomena in addition to regular cytotoxic effects (e.g. vascular remodeling effects and reversal of epithelial to mesenchymal transition [EMT]),[11,12] which have not been reported for vinorelbine, a classic TBD. Our group, as well as others, previously reported the possibility of vascular remodeling by eribulin in preclinical mouse xenograft models and human breast cancer patients with increased microvessel densities (MVD) in the tumors, and enhanced tumor perfusion.[11,13] As the pharmacological outcome of vascular remodeling during eribulin treatment has not been well understood, to further elucidate this, we used a quantitative method that we previously developed to measure tumor perfusion by using radiolabeled liposomes.[14]

Vascular remodeling effects of eribulin can presumably modify the tumor microenvironment. Alteration of tumor microenvironment is expected to improve accumulation of immune cells for effective cancer therapy.[15] Carretero

et al.[16] reported that in a mouse model, the tumor microenvironment altered by vascular normalization increased tumor infiltration of immune cells, such as T cells. Thus, it is important to investigate the relationship between the effect of vascular remodeling and the infiltration of immune cells, and to determine whether these induced immune cells could contribute to the improvement of cancer treatment.

In the present study, we initially investigated a relationship between vascular remodeling effects and antitumor activities of eribulin in multiple human cancer xenograft models. We next evaluated the effects of eribulin-induced vascular remodeling on tumoral accumulation of macromolecular liposomal anticancer agent (i.e. Doxil; Janssen Biotech, Inc., Horsham, PA, USA), as well as recruitment of immune cells into the tumors. We determined that both accumulation of Doxil and recruitment of immune cells were enhanced by eribulin treatment. Collectively, our findings demonstrate that eribulin functions as a microenvironment modulator, and this alteration was advantageous for cancer treatment.

Materials and Methods

Cell lines and culture conditions. Human melanoma cell line LOX was obtained from the National Cancer Institute (Bethesda, MD, USA). Non-small-cell lung cancer (NSCLC) cell lines NCI-H460, NCI-H1650, NCI-H441, NCI-H1993, Calu-6, HCC827, NCI-H1975, A-427, breast cancer cell line MDA-MB 231 and colon cancer cell line HCT116 were obtained from American Type Culture Collection (Andover, MA, USA). NSCLC cell line, A549 was obtained from National Institutes of Biomedical Innovation, Health and Nutrition (Tokyo, Japan). We established HSAEC_4T53RD cell line as described elsewhere.[17] Culture conditions are described in Data S1.

Drugs. Eribulin was manufactured at Eisai. Co. Ltd (Tokyo, Japan). Doxil, the commercial product of PEGylated liposomal agent containing doxorubicin was purchased from Janssen Pharmaceutical K.K. (Tokyo, Japan). Vinorelbine was purchased from Kyowa Hakko Kirin Co. Ltd (Tokyo, Japan).

Human cancer xenograft models. All animal studies were approved by Eisai Institutional Animal Care and Use Committee, as well as the Institutional Animal Experimental Committee at the National Cancer Center. All human cancer cell lines were s.c. transplanted into 6–8-week-old female nude mice (CAnN.Cg-Foxn1nu/CrlCrlj mice; Charles River, Inc., Shizuoka, Japan). Approximately 10–14 days after transplantation, drug administration at the indicated doses and time points was started. Tumor volume (TV) as well as bodyweight was measured at least twice a week. TV was calculated according to the following formula:

$$TV\,(mm^3) = length\,(mm) \times width\,(mm) \times width\,(mm) \times \frac{1}{2}.$$

Relative TV (RTV) was calculated according to the following formula:

$$RTV = \frac{TV\ on\ day\ n}{TV\ on\ first\ day\ of\ drug\ administration}$$

As a parameter of the antitumor effects of eribulin, $\Delta T/C$ (% of control for Δ growth) was calculated from the formula: $(\Delta T/\Delta C) \times 100$. ΔT and ΔC are interval (or longitudinal) changes in tumor volume (Δ growth) for treated and vehicle control groups, respectively. Details were described previously.[18]

Immunohistochemical staining of CD31 and alpha-smooth muscle actin (α-SMA). Tumors were fixed with IHC Zinc Fixative (BD Pharmingen, San Diego, CA, USA). Paraffin-embedded tissues were used for staining of CD31 and α-SMA. Samples were sectioned (8–10 μm), mounted on positively charged slides, and air-dried for 30 min. Sections were deparaffinized and rehydrated in PBS (pH 7.4). After PBS rinses, the sections were incubated at 4°C with rat anti-mouse CD31 antibody (BD Pharmingen) or rabbit anti-mouse α-SMA antibody (Abcam, Cambridge, MA, USA) overnight, and then incubated for 30 min at room temperature with Histofine® Simple Stain™ Mouse MAX PO (for rat IgG) or Histofine® Simple Stain™ AP (R) (for rabbit IgG) (Nichirei Bioscience, Inc., Tokyo, Japan). Brown color was developed by incubating with diaminobenzidine solution for 1 min at room temperature. For quantification of MVD and α-SMA-positive areas in the sections stained for CD31 and α-SMA, all tumor regions were selected, except for the necrotic region, at 20× magnification and measured for each sample. CD31 and α-SMA-positive areas were analyzed by using inForm® 2 software (PerkinElmer Inc., Waltham, MA, USA).

Preparation of ^{111}In-labeled PEGylated liposomes. PEGylated liposomes encapsulating ^{111}In-diethylene-triamine-penta-acetic acid (^{111}In-DTPA) were prepared by the lipid film hydration extrusion method as described previously.[14,19] In brief, the dried films were dispersed in 50 mM HEPES buffer (pH 7.4) containing 5% mannitol and 10 mM DTPA at 60°C and then repeatedly extruded through polycarbonate membrane filters (0.4-, 0.2- and 0.05-μm pore sizes) (GE Healthcare, Buckinghamshire, UK) to adjust their diameters to approximately 80 nm. Unencapsulated DTPA was removed by passage through a Sephadex G-50 column (GE Healthcare Japan Ltd, Tokyo, Japan). Phospholipid concentration was measured by phospholipid assay (Wako Pure Chemical Industries, Ltd, Osaka, Japan). Liposomes were then labeled with ^{111}In (Nihon Mediphysics Co. Ltd, Chiba, Japan). To achieve a high level of specific radioactivity, a remote loading method was used; specifically, ^{111}In was loaded inside the liposomes through the liposomal membranes by transchelation between lipophilic oxine and hydrophilic DTPA ligands. To determine the diameter of liposomes, we used a dynamic light scattering method (DelsaNano; Beckman Coulter, Fullerton, CA, USA).

***Ex vivo* biodistribution of ^{111}In-labeled PEGylated liposomes.** PEGylated liposomes containing ^{111}In-DTPA (400–600 kBq/2 μmol phospholipids per 200 μL saline) were injected i.v. into tumor-bearing nude mice. After injection, we obtained blood, tumors and other major organs, and measured radioactivities of these specimens by gamma counter (PerkinElmer, Hopkinton, MA, USA) at the indicated time points.

Depletion of NK cells and NK staining. For depletion of NK cells, we used a common and validated method.[20] Briefly, rabbit anti-mouse asialo GM1 (200 μL/1:10 dilution of original stock; Wako Chemicals, Tokyo, Japan was given by tail vein injection every 4 days for five injections starting on day 4 before the beginning of administration of antitumor agents. For subsequent detection of infiltrating CD11b-positive cells and NK cells in the tumor, APC-conjugated rat anti-mouse CD11b antibody (Pharmingen BD Biosciences, Tokyo, Japan) or anti-rabbit NCR1 antibody (Abcam, Tokyo, Japan) were used with frozen tissue and paraffin-embedded tissues, respectively. To quantitatively evaluate infiltrating immune cells, images of at least five randomly selected tumor areas were acquired under 20× magnification (0.14 mm^2). Percentage of stained area to total image

area was assessed by computer-aided image analysis with inForm® 2 software (PerkinElmer Inc.). Mean values of the five measured areas of each tumor were calculated, and the subsequent results are shown as the mean of five tumors per group.

Statistical analysis. All data are expressed as mean ± SD. Tukey's multiple comparison test and Student's *t*-test were used to evaluate statistical significance between control and treatment groups with relation to CD31-positive MVD and effect of NK cell depletion. All *P*-values represent two-sided tests of statistical significance. Combination effect was evaluated by using two-way ANOVA. In every analysis, $P < 0.05$ was considered statistically significant. Statistical analyses were carried out using GraphPad Prism version 6.07 (GraphPad Software Inc., La Jolla, CA, USA).

Results

Significance of vascular remodeling effects induced by eribulin for antitumor activities. We initially investigated antitumor activities of eribulin (1.5 mg/kg, 1 shot) in 10 multiple xenograft models including lung cancer, melanoma, as well as colon cancer, and found various pharmacological effects of

this anticancer agent. Eribulin treatment showed tumor regression (maximum RTV < 1) and growth delay effect in seven and two human cancer xenograft models, respectively. Eribulin did not show antitumor effect in the H460 xenograft model (Fig. 1a).

To investigate whether eribulin treatment would increase MVD in these models, tumors were isolated 7 days after treatment and stained with CD31 antibody. Immunohistochemical staining suggested significant enhancement of MVDs in six out of 10 xenografted tumors by eribulin treatment (Fig. 1b,c).

Next, we analyzed the correlation between eribulin-induced enhancement of MVD and antitumor activities of eribulin in these xenograft models. We determined that there was a correlation between enhanced MVD and antitumor effects ($R^2 = 0.54$) (Fig. 1d). Among the tumors examined, A427, an outlier of the correlation curve was further analyzed histologically by CD31 staining. Histological analysis revealed that tumor vessels of A427 were located in the limited stromal region when compared with H1975 xenografted tumor, implying that although MVD were increased after eribulin treatment, drug accumulation was limited in the A427 tumor (Fig. 1c; Fig. S1).
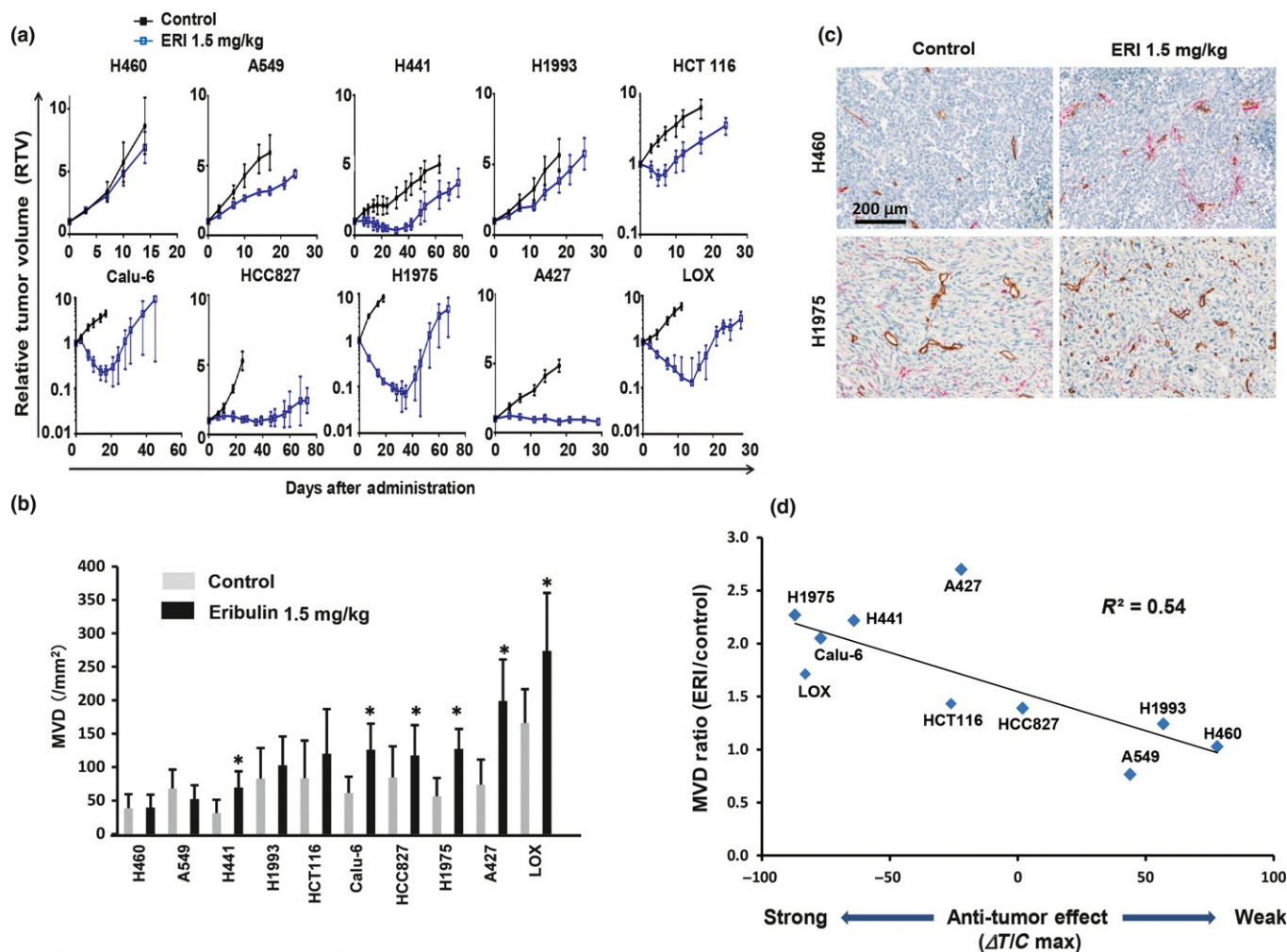

Fig. 1. A critical factor associated with vascular remodeling effect induced by eribulin in multiple human cancer xenograft models. Increase of microvessel density (MVD) was defined as a parameter for vascular remodeling effect of eribulin. Eribulin (ERI, 1.5 mg/kg) was given to mice at day 0 by tail vein injection. (a) Antitumor effects of eribulin in 10 human cancer xenograft models ($n = 6$ for each group). (b) MVD at 7 days after treatment of eribulin in 10 human cancer xenograft models ($n = 3$). (c) Representative immunohistochemical staining with CD31 (tumor vessel) and alpha-smooth muscle actin (α-SMA) (pericyte) in H460 and H1975 xenografted tumors. Majority of vessels were not covered by pericytes. Brown, CD31, red, α-SMA. (d) Correlation between enhancement of vascular remodeling (MVD) and antitumor effects of eribulin. *$P < 0.05$.

To test whether eribulin treatment would enhance MVD in a xenograft model that is more closely related to a cancer patient, we examined MVD in the human breast cancer patient derived xenograft model (PDx). Indeed, we confirmed enhanced MVD in the PDx model after treatment with eribulin (Fig. S2). These results suggested that increased tumor vessels showed modest positive effects on the antitumor activity of eribulin in the xenografted tumors.

Superior vascular remodeling effects and antitumor activities of eribulin over vinorelbine in HSAEC_4T53RD, H1650, and PE-H1650 xenograft models. To clarify the significance of eribulin-induced vascular remodeling effects, we investigated the vascular remodeling effects of another TBD, vinorelbine. Specifically, we measured MVD with CD31 staining in nude mice bearing human NSCLC, HSAEC_4T53RD, H1650, and post-erlotinib treatment H1650 (PE-H1650) xenografted tumors after treatment with eribulin (2 mg/kg, Q4D2) or vinorelbine (15 mg/kg, Q4D2) (all doses given were maximum tolerated doses). Tumors were isolated 7 days after initial drug administration based on the previous experiment showing increased MVD.[11] Immunohistochemical staining of three xenografted tumors showed that eribulin treatment, but not vinorelbine, significantly increased MVD (Fig. 2). Furthermore, we confirmed that eribulin treatment increased perfusion/permeability by Hoechst staining assay in a HSAEC_4T53RD xenograft model, which suggested that eribulin-induced tumor vessels were functional (Fig. S3). We next examined *in vivo* antitumor activities of the anticancer agents. Consistent with increased MVD in the xenografted tumors, eribulin had stronger antitumor effects than vinorelbine (Fig. 3). These results indicated unique characteristics of eribulin presumably as a result of its vascular remodeling effect.

Eribulin treatment, but not vinorelbine, increased accumulation of radiolabeled PEGylated liposomes and enhanced antitumor activities of Doxil in PE-H1650 xenografted tumors. To confirm increased tumor perfusion by eribulin, we measured accumulation of radiolabeled liposomes with an average diameter of 85.0 nm ($n = 3$ independent experiments) in the tumor. Eribulin or vinorelbine was i.v. injected, followed by injection of the radiolabeled liposomes 3 days later. Then, we determined biodistribution patterns of ^{111}In-labeled PEGylated liposomes at 48 h after injection in the PE-H1650 xenograft model. Accumulation levels of ^{111}In-labeled PEGylated liposomes in the eribulin-treated tumors were significantly higher than in vinorelbine-treated tumors at 48 h after injection of radiolabeled liposomes (Fig. 4a). Conversely, we did not observe different accumulation patterns in major organs and tissues among these groups (Table S1).

To clarify whether increased liposomal accumulation in the tumor, which was induced by eribulin, was advantageous for cancer treatment, we next investigated *in vivo* antitumor effects of Doxil, a liposomal anticancer agent, after treatment with either eribulin or vinorelbine in the PE-H1650 xenograft model. Eribulin (1 mg/kg) or vinorelbine (7.5 mg/kg) was given to mice by tail vein injection. At 3 days after administration, Doxil (10 mg/kg) was i.v. injected into the mice. Eribulin, but not vinorelbine, synergistically enhanced antitumor effects of the subsequent Doxil treatment ($P < 0.05$) without severe bodyweight loss (Fig. 4b; Fig. S4). In contrast, Doxil treatment followed by eribulin did not enhance antitumor effects compared to each single treatment. We did not observe enhancement of antitumor activities of vinorelbine followed by Doxil (Fig. 4b). Furthermore, we examined another anticancer agent, paclitaxel, and determined that the combined antitumor effect of paclitaxel was observed only after eribulin treatment in MDA-MB-231 human breast cancer xenograft model (Fig. S5). These results suggest that increased tumor perfusion through the eribulin-induced vascular remodeling effect is crucial for its antitumor effects *in vivo*.

Contribution of immune cells for antitumor activities of eribulin. We finally examined whether eribulin-induced vascular remodeling might increase the number of infiltrating immune cells into the tumor. Contribution of host immune cells to the therapeutic effects of eribulin was analyzed in three NSCLC
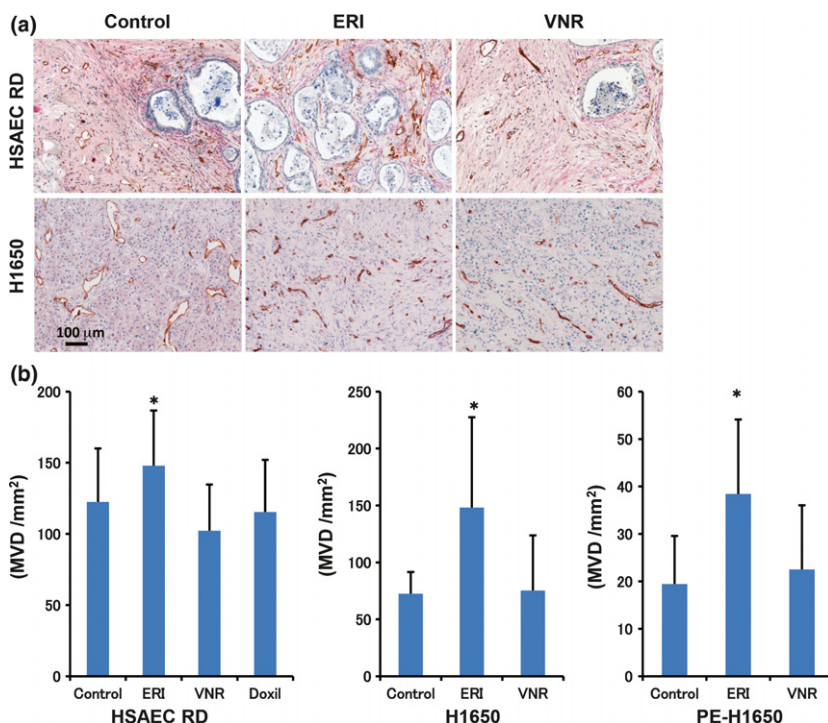

Fig. 2. Vascular remodeling effect of eribulin, but not vinorelbine, in human cancer cell xenograft models. Eribulin (ERI) and vinorelbine (VNR) were given by tail vein injection with Q4D2 schedule. Two days after the last administration of the anticancer agents, tumors were harvested and stained with CD31 and alpha-smooth muscle actin (α-SMA) antibodies. (a) Representative immunohistochemical staining with CD31 and α-SMA in the HSAEC_4T53RD (HSAEC RD) and H1650 xenografted tumors. Brown, CD31, red, α-SMA. (b) MVD in the xenografted tumor ($n = 4$). *$P < 0.05$.
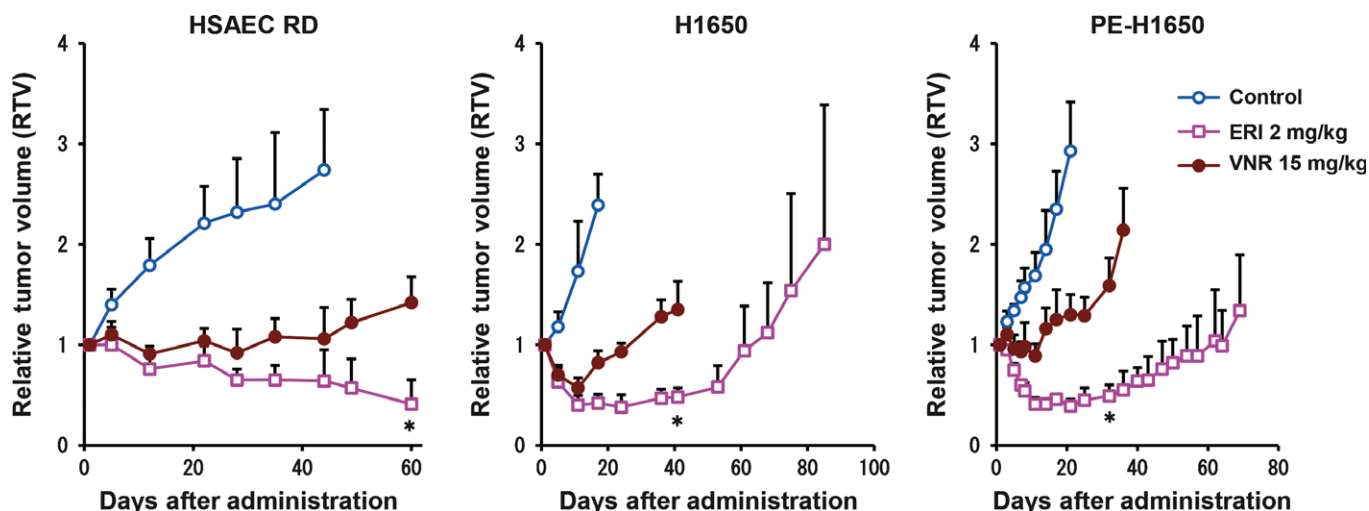
Fig. 3. Comparison of antitumor effects of tubulin targeted agents, eribulin and vinorelbine in the xenograft models. *In vivo* antitumor activities of two tubulin inhibitors (*n* = 6, each group). Eribulin (ERI) at 2 mg/kg and vinorelbine (VNR) at 15 mg/kg (both maximum tolerable doses [MTD]) were given to mice by tail vein injection (Q4D2 schedule). Graphs show antitumor effects of eribulin and vinorelbine in the HSAEC_4T53RD (HSAEC RD), H1650, and post-erlotinib treatment H1650 (PE-H1650) xenograft models. Experiments were carried out twice independently.
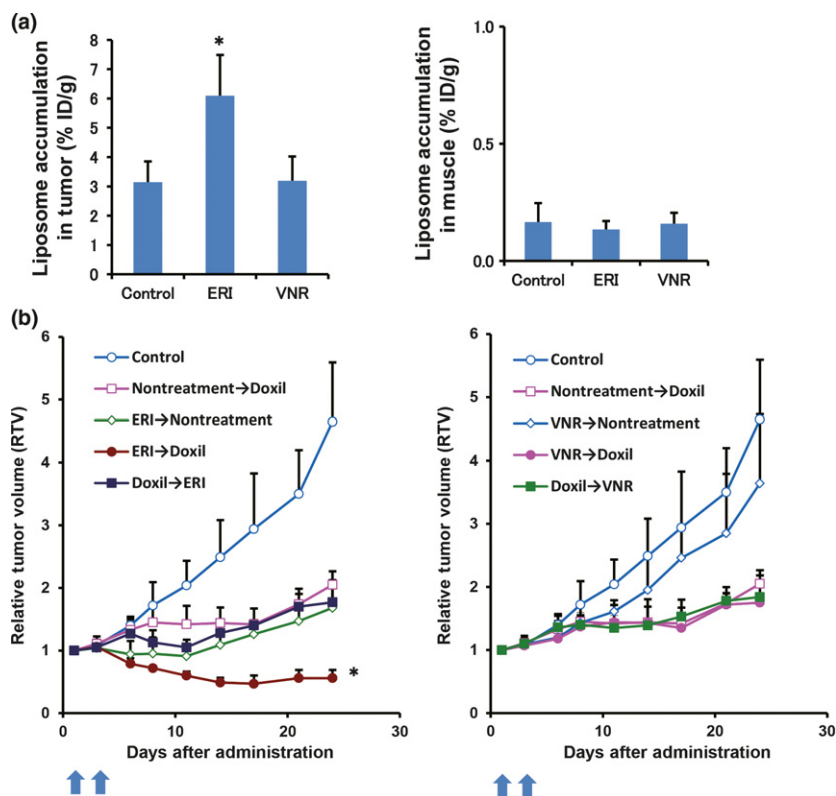

Fig. 4. Eribulin treatment increased accumulation of PEGylated liposomes and enhanced antitumor effects of Doxil (Janssen Pharmaceutical K.K.) in the post-erlotinib treatment H1650 (PE-H1650) xenograft models. (a) Accumulation levels of liposomes in the tumor were measured by radiolabeled liposomes. Graph shows accumulation of ^{111}In-labeled PEGylated liposomes in the tumor. The radiolabeled liposomes were injected 3 days after giving drugs. Muscle was collected as a negative control. (b) *In vivo* antitumor activities of tubulin-targeted agents and Doxil with several regimens in the PE-H1650 xenograft model (*n* = 6, each group). *P < 0.05, eribulin compared with other groups. ERI, eribulin; VNR, vinorelbine.

xenografted tumors. Eribulin treatment enhanced infiltrating host immune cells (CD11b+) when compared to vinorelbine and control groups in three NSCLC, H1650, PE-H1650, and HSAEC_4T53RD tumors (Fig. 5a,b). We also confirmed that infiltrating NK cells were significantly increased by NCR1 staining, which is a specific antibody for NK cells (Fig. S6). Furthermore, we confirmed that depletion of NK cells significantly reduced the antitumor effect of eribulin in the human melanoma (LOX) xenograft model (Fig. 5c), which

demonstrated the highest increase of MVD as illustrated in Figure 1b. These results implied that immune cells infiltrated by vascular remodeling effects of eribulin could contribute to enhancement of antitumor activities.

Discussion

In the present study, we explored whether eribulin-induced vascular remodeling is favorable during cancer treatment in
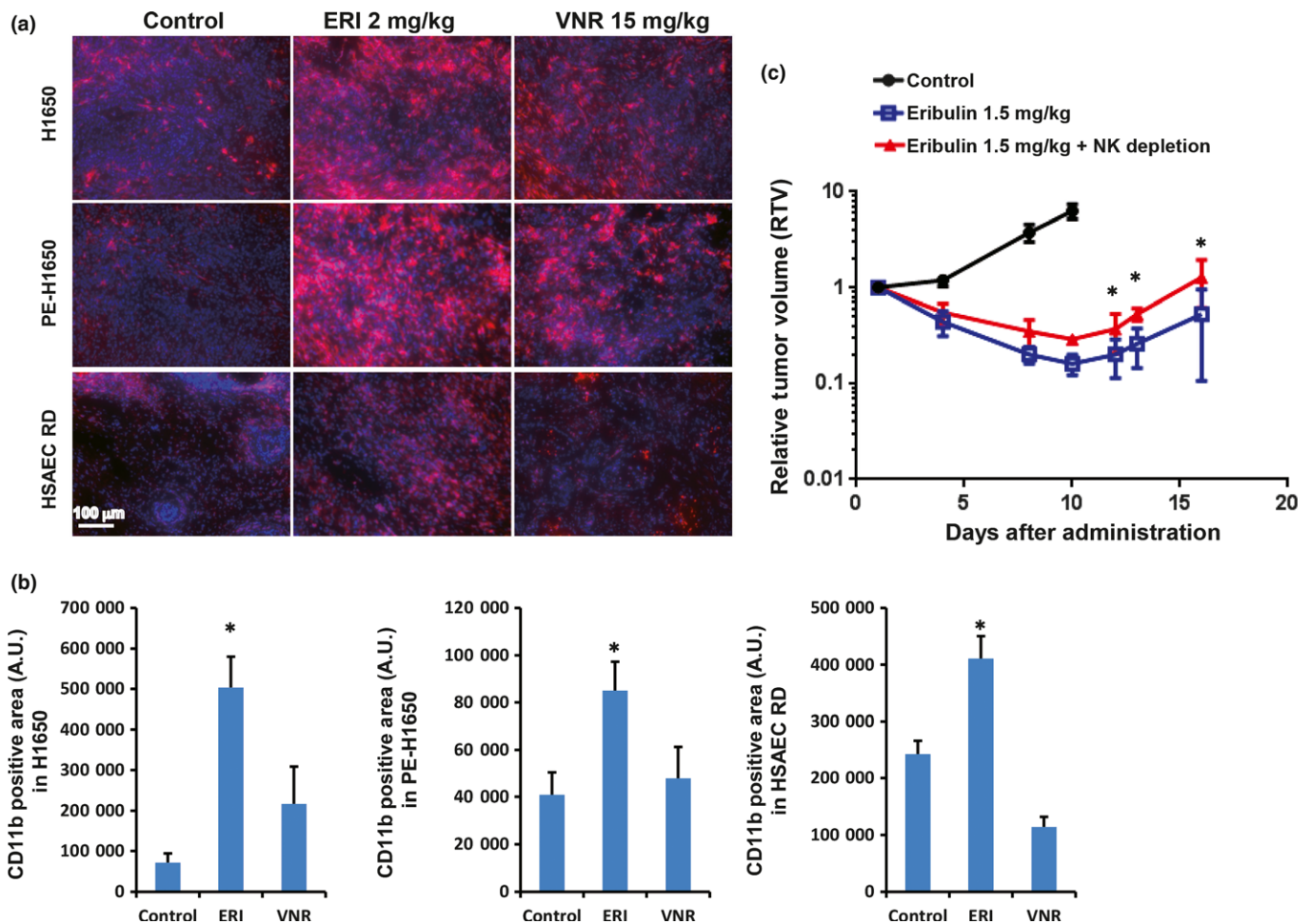
Fig. 5. Contribution of immune cells for antitumor activities of eribulin. Two days after the last administration of the anticancer agents, tumors were harvested and stained with CD11b antibody. (a) Representative images of infiltrating host immune cells into the non-small-cell lung cancer (NSCLC) xenografted tumor. Red, CD11b$^+$ immune cells (monocyte, NK etc.); blue, Hoechst staining (nucleus). (b) Graph shows CD11b$^+$ area in the xenografted tumor. (c) Comparison of antitumor effects of eribulin with or without NK cell depletion in a LOX melanoma xenograft model (n = 7). ERI, eribulin; NK, natural killer cells; VNR, vinorelbine. *P < 0.05.

multiple xenograft models, and found it advantageous based on the following points. (i) There was a correlation between increased MVD in the tumors and antitumor effects of eribulin in 10 human cancer xenograft models, demonstrating the impact of eribulin-induced vascular remodeling effects on anti-tumor activity. (ii) Eribulin treatment, but not vinorelbine, showed vascular remodeling effects, and eribulin exhibited superior antitumor effects over vinorelbine in the three xeno-graft models. (iii) Eribulin treatment, but not vinorelbine, increased accumulation of radiolabeled liposomes in the tumor and showed synergistic antitumor effect of Doxil only after treatment with eribulin. (iv) Eribulin treatment increased infiltrating immune cells in the xenografted tumors, and NK cell depletion significantly reduced antitumor activity. (v) Eribulin treatment increased perfusion in the tumor and reduced hypoxic region (Figs S7,S8). Collectively, these results indi-cate that the vascular remodeling effect of eribulin strongly contributes to its antitumor effects in addition to a classic cyto-toxic effect against tumor cells in preclinical human cancer xenograft models.

Tumor microenvironment consists of multiple factors (e.g. induction of hypoxia, increase of tumor interstitial fluid pres-sure etc.) that can affect the pharmacological effectiveness of anticancer agents on neoplastic cells.[21] It is important to alter

the tumor microenvironment to allow adequate delivery and retention of these agents, consequently leading to improved therapeutic outcomes. One such treatment strategy is vascular normalization, a concept for treatment of cancer patients through enhanced delivery and efficacy of anticancer therapeu-tics.[22] Indeed, normalization of the microenvironment can improve treatment outcomes in mice and patients with malig-nant and non-malignant diseases without increased MVD.[23–26] Although tumor vascular remodeling illustrated here is sim-ilar to vascular normalization in that both strategies alter the tumor microenvironment for enhanced pharmacological out-comes of anticancer agents, there are distinct functional differ-ences between the vascular remodeling effect that is induced by eribulin and vascular normalization.

Comparing vascular normalization and vascular remodeling, one of the current validated mechanisms of vascular normal-ization is blockage of vascular endothelial growth factor (VEGF) signaling.[24] Inhibition of VEGF by bevacizumab, which promotes proliferation and survival of endothelial cells and increases permeability, can transiently restore the balance between pro- and anti-angiogenic signaling, shifting it back towards equilibrium. Thus, vascular normalization by inhibit-ing VEGF signaling has a transient effect. Importantly, the benefit of combination treatment was schedule-dependent (i.e.
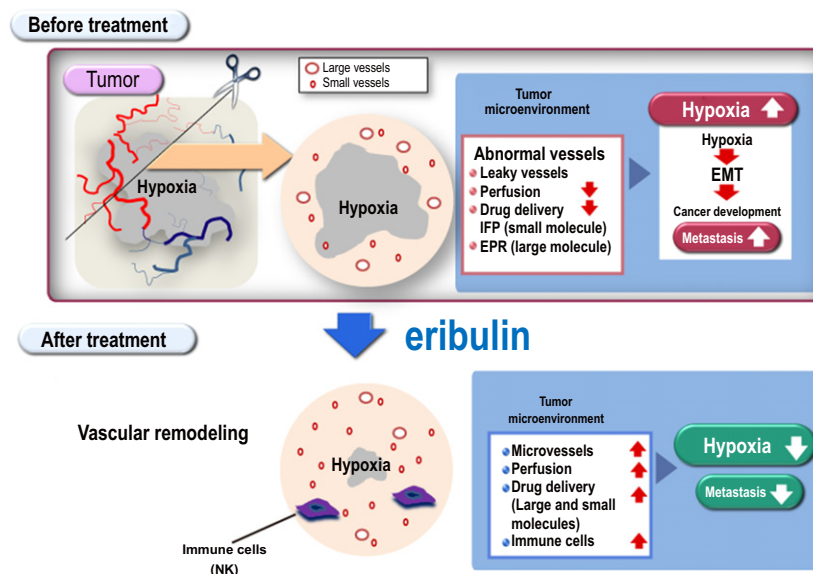
Fig. 6. Role of eribulin as a tumor microenvironment modulator. Merits of the vascular remodeling effect are summarized in the schema. Our cumulative experimental results demonstrate that eribulin functions as a microenvironment modulator through increased drug accumulation (e.g. small molecule by reduced interstitial fluid pressure [IFP] and large molecule by enhanced permeability and retention [EPR] effect), increased infiltrating immune cells, as well as reduced hypoxic region. Collectively, these findings illustrate the significance of eribulin-induced vascular remodeling effect for cancer treatment in multiple mouse xenograft models. EMT, epithelial to mesenchymal transition.

maximum tumor shrinkage was observed when bevacizumab therapy was carried out 3 days before chemotherapy), suggesting that enhancement of chemotherapy specifically occurred when given during the appropriate time period termed "normalization window".[25,27] In contrast, vascular remodeling is expected to provide a long-lasting effect because of stable alterations based on increased number of tumor vessels. Furthermore, Ueda *et al.* recently reported functional differences between vascular normalization with bevacizumab treatment and vascular remodeling with eribulin treatment by *in vivo* imaging of breast cancer patients. Indeed, eribulin treatment, but not bevacizumab, significantly decreased deoxyhemoglobin (HHb) concentration and increased oxyhemoglobin (SO$_2$) during the observation period.[13] These results clearly demonstrated the distinct functional differences between vascular remodeling and vascular normalization.

Based on the basic components of vascular remodeling, as well as evidence we provided herein, eribulin treatment may be advantageous for sequential treatment not only with small compounds but also with macromolecular agents. We previously reported that cytotoxic agents were effective after treatment with eribulin.[11] In this study, eribulin-induced vascular remodeling also increased accumulation of a liposomal anticancer agent, Doxil, in contrast with vascular normalization induced by VEGF blockage that only increased tumor delivery of intermediate size (12 nm) but not larger nanoparticles.[28] Recently, Daldrup-Link *et al.*[26] reported that inhibition of type I transforming growth factor beta (TGF-β) receptor increased the delivery of macromolecules by increased transendothelial permeability in the tumor. Eribulin reduced TGF-β1, a ligand of type I TGF-β receptor expression in both animal models and breast cancer patients, which suggested increased permeability to endothelial cells.[11,13] Furthermore, our histological analyses demonstrated that eribulin treatment did not increase pericyte-covered vessels (Figs 1c,2a). These findings illustrate that vascular remodeling induced by eribulin increased accumulation of macromolecules such as liposomes through an enhanced permeability and retention (EPR) effect and contributed to alter the tumor microenvironment.

Although we described a treatment benefit of eribulin by vascular remodeling, the mechanism of vascular remodeling is not fully understood in this study. It is crucial to elucidate the

mechanism to understand cancer biology. Accumulating reports have shown that eribulin treatment reduced proangiogenic factors, such as VEGF, platelet-derived growth factor (PDGF), basic fibroblast growth factor (bFGF), and MMP in either preclinical models or in cancer patients.[11,13] These results implied that the eribulin-induced vascular remodeling effect did not depend on upregulation of proangiogenic factors.

Last, we also demonstrated that eribulin enhanced accumulation of CD11b+ immune cells, NK cells by staining with NCR 1 antibody (Fig. S6), and depletion of NK cells by antibody reduced antitumor effects of eribulin. These findings suggest a contribution of host immune cells for antitumor effects of eribulin, which is further supported by preclinical evidence demonstrating increased infiltration of CD8$^+$ T cells by vascular normalization.[16] However, protumor effects of CD11b+ cells have also been reported because CD11b+ cells function both as M1-like (tumor suppressive) and M2-like (protumor effect) tumor-associated macrophages (TAM).[16] However, a potential for the induction of M2-like TAM by vascular remodeling seems minimal as eribulin treatment reduced expression levels of VEGF and TGF-β, both of which are highly expressed in M2-like TAM.[11]

Collectively, our findings described herein indicate that vascular remodeling is applicable to alter the tumor microenvironment (Fig. 6). In conclusion, these cumulative results indicate eribulin as a microenvironment modulator by increased drug accumulation, increased infiltrating immune cells, as well as reduced hypoxic region, and demonstrate the significance of vascular remodeling for cancer treatment in multiple mouse xenograft models.

Acknowledgments

Disclosure Statement

References

1 Jordan MA, Wilson L. Microtubules as a target for anticancer drugs. *Nat Rev Cancer* 2004; **4**: 253–65.

2 Kavallaris M. Microtubules and resistance to tubulin-binding agents. *Nat Rev Cancer* 2010; **10**: 194–204.

3 Parker AL, Kavallaris M, McCarroll JA. Microtubules and their role in cellular stress in cancer. *Front Oncol* 2014; **4**: 153.

4 Brouhard GJ, Rice LM. The contribution of alphabeta-tubulin curvature to microtubule dynamics. *J Cell Biol* 2014; **207**: 323–34.

5 Smith JA, Wilson L, Azarenko O *et al.* Eribulin binds at microtubule ends to a single site on tubulin to suppress dynamic instability. *Biochemistry* 2010; **49**: 1331–7.

6 Capasso A. Vinorelbine in cancer therapy. *Curr Drug Targets* 2012; **13**: 1065–71.

7 Cortes J, O'Shaughnessy J, Loesch D *et al.* Eribulin monotherapy versus treatment of physician's choice in patients with metastatic breast cancer (EMBRACE): a phase 3 open-label randomised study. *Lancet* 2011; **377**: 914–23.

8 Donoghue M, Lemery SJ, Yuan W *et al.* Eribulin mesylate for the treatment of patients with refractory metastatic breast cancer: use of a "physician's choice" control arm in a randomized approval trial. *Clin Cancer Res* 2012; **18**: 1496–505.

9 Pean E, Klaar S, Berglund EG *et al.* The European Medicines Agency review of eribulin for the treatment of patients with locally advanced or metastatic breast cancer: summary of the scientific assessment of the committee for medicinal products for human use. *Clin Cancer Res* 2012; **18**: 4491–7.

10 Schoffski P, Chawla S, Maki RG *et al.* Eribulin versus dacarbazine in previously treated patients with advanced liposarcoma or leiomyosarcoma: a randomised, open-label, multicentre, phase 3 trial. *Lancet* 2016; **387**: 1629–37.

11 Funahashi Y, Okamoto K, Adachi Y *et al.* Eribulin mesylate reduces tumor microenvironment abnormality by vascular remodeling in preclinical human breast cancer models. *Cancer Sci* 2014; **105**: 1334–42.

12 Yoshida T, Ozawa Y, Kimura T *et al.* Eribulin mesilate suppresses experimental metastasis of breast cancer cells by reversing phenotype from epithelial-mesenchymal transition (EMT) to mesenchymal-epithelial transition (MET) states. *Br J Cancer* 2014; **110**: 1497–505.

13 Ueda S, Saeki T, Takeuchi H *et al.* In vivo imaging of eribulin-induced reoxygenation in advanced breast cancer patients: a comparison to bevacizumab. *Br J Cancer* 2016; **114**: 1212–8.

14 Umeda IO, Tani K, Tsuda K *et al.* High resolution SPECT imaging for visualization of intratumoral heterogeneity using a SPECT/CT scanner dedicated for small animal imaging. *Ann Nucl Med* 2012; **26**: 67–76.

15 Huang Y, Goel S, Duda DG, Fukumura D, Jain RK. Vascular normalization as an emerging strategy to enhance cancer immunotherapy. *Cancer Res* 2013; **73**: 2943–8.

16 Carretero R, Sektioglu IM, Garbi N, Salgado OC, Beckhove P, Hammerling GJ. Eosinophils orchestrate cancer rejection by normalizing tumor vessels and enhancing infiltration of CD8(+) T cells. *Nat Immunol* 2015; **16**: 609–17.

17 Sasai K, Sukezane T, Yanagita E *et al.* Oncogene-mediated human lung epithelial cell transformation produces adenocarcinoma phenotypes in vivo. *Cancer Res* 2011; **71**: 2541–9.

18 Ito K, Semba T, Uenaka T, Wakabayashi T, Asada M, Funahashi Y. Enhanced anti-angiogenic effect of E7820 in combination with erlotinib in epidermal growth factor receptor-tyrosine kinase inhibitor-resistant non-small-cell lung cancer xenograft models. *Cancer Sci* 2014; **105**: 1023–31.

19 Ito K, Hamamichi S, Asano M *et al.* Radiolabeled liposome imaging determines an indication for liposomal anticancer agent in ovarian cancer mouse xenograft models. *Cancer Sci* 2016; **107**: 60–7.

20 Monnier J, Zabel BA. Anti-asialo GM1 NK cell depleting antibody does not alter the development of bleomycin induced pulmonary fibrosis. *PLoS One* 2014; **9**: e99350.

21 Saggar JK, Yu M, Tan Q, Tannock IF. The tumor microenvironment and strategies to improve drug distribution. *Front Oncol* 2013; **3**: 154.

22 Jain RK. Normalizing tumor microenvironment to treat cancer: bench to bedside to biomarkers. *J Clin Oncol* 2013; **31**: 2205–18.

23 Jain RK. Normalizing tumor vasculature with anti-angiogenic therapy: a new paradigm for combination therapy. *Nat Med* 2001; **7**: 987–9.

24 Jain RK. Normalization of tumor vasculature: an emerging concept in antiangiogenic therapy. *Science* 2005; **307**: 58–62.

25 Goel S, Duda DG, Xu L *et al.* Normalization of the vasculature for treatment of cancer and other diseases. *Physiol Rev* 2011; **91**: 1071–121.

26 Daldrup-Link HE, Mohanty S, Ansari C *et al.* Alk5 inhibition increases delivery of macromolecular and protein-bound contrast agents to tumors. *JCI Insight* 2016; **1**(6): e85608.

27 Turetschek K, Preda A, Novikov V *et al.* Tumor microvascular changes in antiangiogenic treatment: assessment by magnetic resonance contrast media of different molecular weights. *J Magn Reson Imaging* 2004; **20**: 138–44.

28 Chauhan VP, Stylianopoulos T, Martin JD *et al.* Normalization of tumour blood vessels improves the delivery of nanomedicines in a size-dependent manner. *Nat Nanotechnol* 2012; **7**: 383–8.

Supporting Information

Additional Supporting Information may be found online in the supporting information tab for this article:

Data S1. Supplementary materials and methods.

Table S1. Biodistribution patterns of radiolabeled liposomes in the tumor and organs.

Fig. S1. Histological comparison between A427 and H1975 xenograft models.

Fig. S2. Vascular remodeling effect of eribulin in the patient-derived breast cancer xenograft model (PDx).

Fig. S3. Eribulin increased perfusion/permeability in the HSAEC_4T53RD xenograft model.

Fig. S4. Relative bodyweight (RBW) in the PE-H1650 xenograft model.

Fig. S5. Antitumor effect of eribulin followed by paclitaxel treatment in the MDA-MD231 xenograft model.

Fig. S6. Eribulin treatment significantly increased infiltrating natural killer (NK) cells in the H1650 xenograft model.

Fig. S7. Eribulin increased perfusion in the FaDu xenograft model.

Fig. S8. Eribulin reduced hypoxia region in the OSC-19 xenograft model.